Available online at www.sciencedirect.com

jmr&t Journal of Materials Research and Technology

https://www.journals.elsevier.com/journal-of-materials-research-and-technology

Original Article

Phase chemistry of Submerged Arc Welding (SAW) fluoride based slags

Theresa Coetsee

University of Pretoria, Pretoria, South Africa

ARTICLE INFO

Article history:
Received 30 April 2020
Accepted 18 June 2020
Available online 16 July 2020

Keywords:
Welding
Flux
Slag
Phase chemistry
Gas
SAW

ABSTRACT

Phase chemical analysis of post-weld slags from Submerged Arc Welding (SAW) is applied to explain the chemical function of flux constituent compounds in the welding process. FactSage 6.4 calculations were used to aid in the interpretation of the phase chemical analyses. Five commercial agglomerated fluxes from two suppliers were used. These fluxes cover three types of fluoride based flux classes: Fluoride Basic flux, Aluminate Basic flux and Aluminate Rulile flux. Basic fluxes are based in the SiO_2–$Al2O_3$–MgO CaF_2 system. The slag liquidus lowering effect of CaF_2 is 19 °C/%CaF_2 in the Fluoride Basic fluxes, and 4 °C/%CaF_2 in the Aluminate Basic fluxes. The Aluminate Rutile flux is based in the SiO_2–$Al2O_3$–MgO–TiO_2–MnO–CaF_2 system. Little CaF_2 addition is used in this flux since TiO_2 addition lowers its liquidus temperature sufficiently. The level of CaF_2 addition sets the quantity and chemistry of fluoride gas compounds formed. The main gas fluoride gas species expected to form in welding with the five fluxes are CaF_2, MgF_2, NaF, KF, $NaAlF_4$, and AlF_3. In addition, TiF_3 is expected to form in welding with the Aluminate Rutile flux, indicating the importance of titanium oxidation state in fluoride gas formation.

1. Introduction

In Submerged Arc Welding (SAW) the welding flux, weld wire, steel base plate and welding parameters together set the weld metal physical metallurgy properties [1–5]. For example, in SAW of HSLA (High Strength Low Alloy Steels), silicon and manganese are the two main alloying elements in the weld metal that are controlled by setting the welding flux chemistry to increase or maintain the level of silicon and manganese in the weld metal. This is accomplished by specifying the weld flux chemistry for a combination of welding wire and steel base plate. Most fluxes used in SAW contain some quantity of CaF_2 to shield the weld pool from hydrogen, nitrogen and oxygen pickup from atmospheric air, and also to increase the slag hydrogen dissolution capacity and to chemically react with water to form hydrogen fluoride gas [3,5–9]. Oxygen enters the weld metal mainly due to decomposition of less stable oxides such as MgO, SiO_2, MnO, and FeO in the arc cavity to release oxygen gas [3,5]. These reactions are possible due to the high temperatures reached in the plasma of the arc cavity, reported to be at 2000 °C–2500 °C [10,11]. This oxygen gas is adsorbed onto the surface of molten steel droplets that are formed as the weld wire is melted in the arc cavity [12,13]. The addition of fluoride to the flux, usually CaF_2, is used to lower the P_{O_2} in the arc cavity [3,5]. Similarly, the P_{H_2} is lowered to limit hydrogen pickup into the weld metal [3,6,8].

E-mail: theresa.coetsee@up.ac.za

https://doi.org/10.1016/j.jmrt.2020.06.069

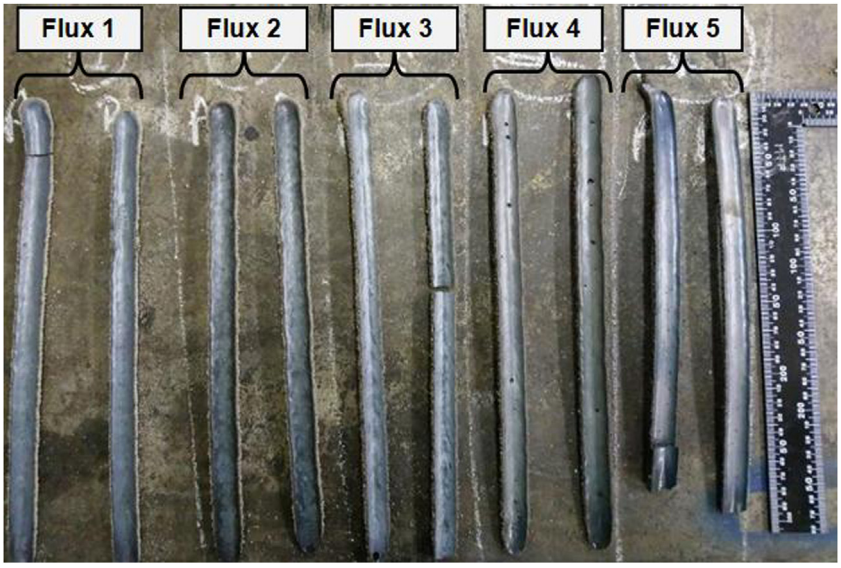

Fig. 1 – Post-weld slag samples.

Table 1 – Base plate and weld wire chemical composition (mass percentages).

	C	O	Si	Mn	Al	P	S	Ti	Cu
Plate	0.120	0.007	0.155	1.340	0.067	0.019	0.007	0.005	0.030
Wire	0.110	0.003	0.137	0.990		0.009	0.023		0.140

In addition to the above reasons for adding CaF_2 to fluxes, there are several important chemical actions of CaF_2 in setting physico-chemical properties of the molten flux (slag), such as the significant lowering of slag melting temperatures, lowering the slag viscosity and surface tension since CaF_2 serves as a slag network modifier. Despite the clear importance of CaF_2 in flux formulations, its role in weld slag chemistry is complex. For example, it was argued that CaF_2 should be removed as a basic flux compound in the widely used flux basicity index (BI) since it is a neutral compound in the slag [2]. $BI = [CaF_2 + CaO + MgO + BaO + SrO + Na_2O + K_2O + Li_2O + 0.5(MnO + FeO)]/[SiO_2 + 0.5(Al_2O_3 + TiO_2 + ZrO_2)]$. An important empirically determined composition guideline is to ensure that the flux BI is in excess of 1.5 to ensure low hydrogen and low total oxygen content in the weld metal [2]. It was shown that CaF_2 alone lowers weld metal oxygen content, and since most of the CaF_2 remains in the slag as CaF_2 it is important to include this compound in the BI expression [7]. Most of the published literature on welding is focussed on weld metal composition and its relation to weld metal physical metallurgy properties. Only a few published studies reported post-weld slag compositions and/or slag properties for SAW, or from similar welding techniques [6,14–20]. Therefore, limited information on flux formulations and the chemical function of each flux constituent compound is published, mostly due to protection of industry commercial interests [9].

The objective of this work is to use post-weld slag phase chemistry to interpret the chemical functional basis of fluoride flux formulations used in SAW as presented in the fluxes used in this study. Five commercial agglomerated fluxes from two suppliers were used in SAW welding, and the post-weld slag analysed by using mineralogy techniques. Slag phase chemistry is discussed with the aid of FactSage 6.4 thermochemical calculations [21].

2. Materials and methods

Each commercial agglomerated SAW flux was used to make two bead-on-plate welds and the post-weld slags were collected for phase chemical analyses, see Fig. 1. Weld heat input was 2.0 kJ/mm (500 A, 28 V, 42 cm/min) welded DCEP + with 3.2 mm diameter wire. Structural steel grade EN 10025-2 was used as base plate material. The chemical analyses of the steel consumables are summarised in Table 1. The base plate steel was analysed by Optical Emission Spectroscopy (OES) and oxygen content in the base plate and weld wire was analysed by combustion method. The weld wire major element levels are from the manufacturer's specification.

Bulk chemical analyses and X-ray diffraction (XRD) analyses were applied to each raw flux and post-weld slag sample. Bulk chemistry analyses were done by Inductively Coupled Plasma Optical Emission Spectrometry (ICP-OES), and titration method for fluorine analyses. The phase chemistry in each post-weld slag sample was measured by Scanning Electron Microscopy (SEM). These analyses were specifically made at the slag surface which was in contact with the weld metal during welding since the slag-weld pool interface is the reaction interface where the final chemical reactions in welding occur. Therefore, comparison of the slag SEM analyses at this interface to the bulk slag chemistry would show up any major composition differences that occurred due to the welding process.

Table 2 – Crystalline phases present in flux (mass percentages).

Flux type		Fluoride basic	Aluminate basic	Fluoride basic	Aluminate basic	Aluminate rutile
Flux number		1	2	3	4	5
Fluorite	CaF_2	36.6	32.0	29.5	21.7	3.2
Corundum	Al_2O_3	24.6	17.2	16.6	20.2	54.4
Periclase	MgO	32.8	36.6	41.1	33.3	7.7
Calcite	$CaCO_3$	0	1.3	3.2	0	0
Wollastonite	$CaSiO_3$	3.3	8.4	6.1	0	4.4
Mullite	$Al_{4.52}O_{9.74}Si_{1.48}$	0	0	1.4	17.4	7.3
Quartz	SiO_2	1.3	1.3	2.1	1.5	2.7
Cristobalite	SiO_2	0	0	0	1.8	0
Kyanite	$Al_2O_3SiO_2$	0	0	0	4.1	0
Jacobsite	Fe_2MnO_4	0	0	0	0	2.2
Manganosite	MnO	0	0	0	0	1.6
Mn	Mn	0	0	0	0	3.1
Zircon	ZrSiO4	0	0	0	0	4.3
Rutile	TiO_2	1.3	0.3	0	0	9.1
Forsterite	$Mg_{1.834}Fe_{0.155}Ni_{0.011}SiO_4$	0	2.9	0	0	0
BI		3.0	1.8	2.9	1.4	0.5

Table 3 – Flux compositions (mass percentages).

Flux number	1	2	3	4	5
MnO	0.87	5.83	1.11	6.80	12.30
CaO	24.20	19.90	25.30	12.50	5.27
Al_2O_3	13.90	17.30	17.90	24.90	36.0
SiO_2	15.10	21.30	13.40	19.60	18.60
MgO	32.10	21.20	29.80	22.20	4.94
Fe_2O_3	0.65	1.01	1.10	2.67	5.97
TiO_2	0.74	1.86	1.18	0.97	10.70
ZrO_2	0.01	0.01	0.03	0.02	0.24
Na_2O	2.00	2.69	1.57	1.61	2.20
K_2O	0.78	1.50	1.15	0.18	0.51
P	0.018	0.031	0.015	0.025	0.033
S	0.033	0.028	0.013	0.018	0.020
F	12.5	11.0	12.6	8.41	2.04
Ba	0.070	0.081	0.017	0.037	0.048
Cr	0.011	0.015	0.010	0.026	0.073
Cu	0.008	0.008	0.005	0.007	0.011
Ni	0.021	0.011	0.003	0.010	0.022
Sr	0.023	0.053	0.006	0.006	0.010
V	0.012	0.013	0.008	0.011	0.031
Moisture	0.020	0.040	0.020	0.000	0.000
Total	103.2	103.9	105.6	100.1	99.1
BI	3.0	1.8	2.9	1.4	0.5

The XRD samples were prepared according to the standardized Panalytical backloading system, which provides nearly random distribution of the particles. The samples were analyzed using a PANalytical X'Pert Pro powder diffractometer in θ–θ configuration with an X'Celerator detector and variable divergence- and fixed receiving slits with Fe filtered Co–Kα radiation (λ = 1.789 Å). The mineralogy was determined by selecting the best–fitting pattern from the ICSD database to the measured diffraction pattern, using X'Pert Highscore plus software. The relative phase amounts (mass% of crystalline portion) were estimated using the Rietveld method (Autoquan Program). SEM analyses were done at 20 kV acceleration voltage and using 40 s count time using a JEOL-IT300 SEM–EDS with Oxford X-max 50 detector.

XRD analyses of the fluxes are summarised in Table 2 and the corresponding bulk chemical analyses are displayed in Table 3. According to typical commercial classification names used, fluxes 1 and 3 are Fluoride Basic fluxes, fluxes 2 and 4 are Aluminate Basic fluxes, and flux 5 is an Aluminate Rutile flux, [9]. Fluxes 1–4 contain CaF_2, Al_2O_3 and MgO as the main crystalline compounds with minor quantities of quartz and synthetic silicates of mullite and wollastonite. Flux 5 contains Al_2O_3 as the main crystalline compound, and it also contains smaller quantities of CaF_2, MgO, quartz and synthetic silicates with significant quantities of TiO_2 and manganese compounds. Amorphous water glass is used as binding agent in the preparation of agglomerated fluxes, therefore the total mass% SiO_2 in the bulk chemical analyses of the

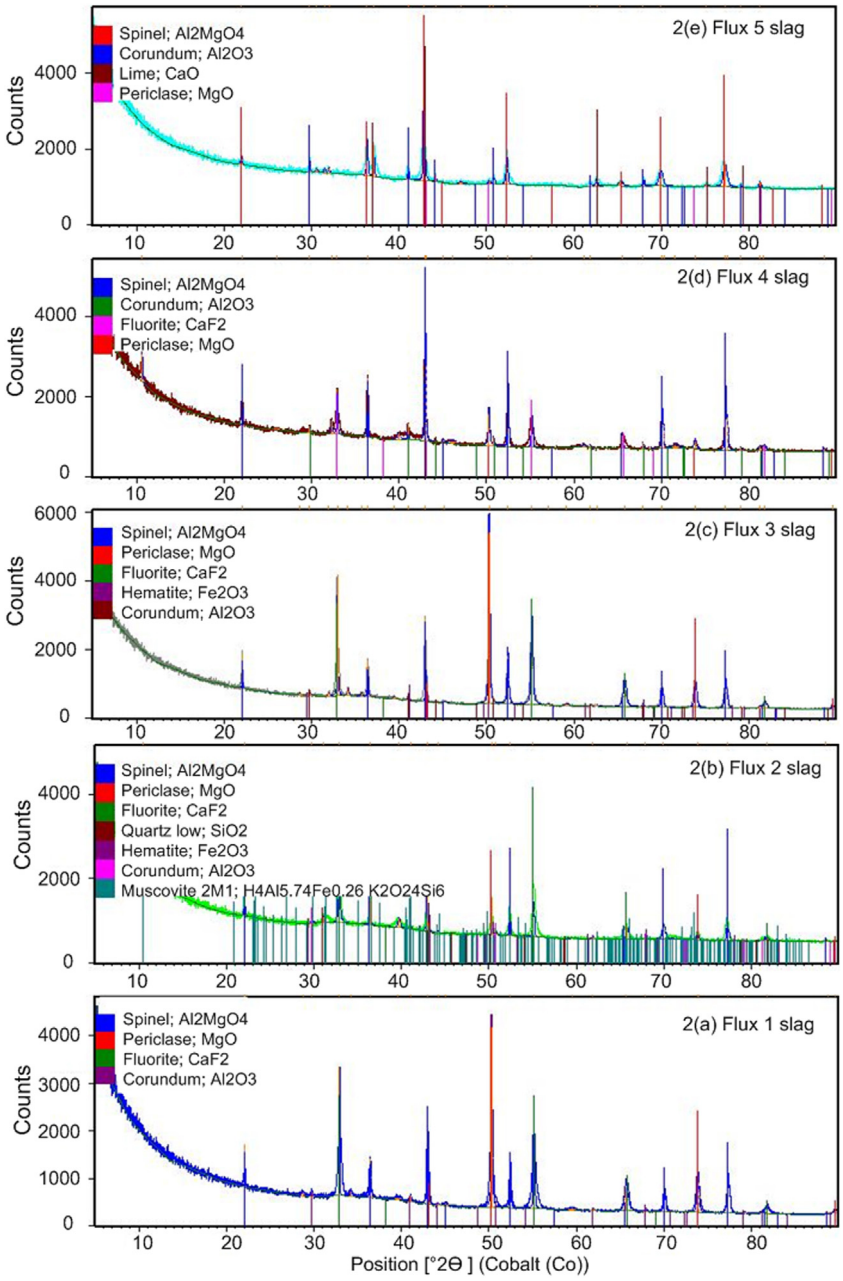

Fig. 2 – Slag XRD analyses patterns.

fluxes (Table 3) are higher that that presented by the crystalline phases in Table 2.

3. Results

Crystalline phases were identified in the XRD analyses of all the post-weld slags as displayed in Fig. 2(a)–(e). The characteristic hump in the count rate values at low 2Θ values indicates the presence of amorphous phases, and was seen in all the slag XRD patterns as displayed in Fig. 2(a)–(e). All of the fluxes contain CaF_2, MgO and Al_2O_3 and these compounds are also identified in the bulk slag XRD analyses because the top surface of the slag still contains some partially molten flux material. Some of the MgO and Al_2O_3 reacted to form spinel ($MgO{\cdot}Al_2O_3$) in the slag. This is the case for all the post-weld slag XRD analyses in Fig. 2.

Fig. 3(a)–(e) display the typical phase assembly and chemistry in each post-weld slag sample as analysed by SEM. Phase analyses of the phases displayed in Fig. 3(a)–(e) are summarised in each accompanying table (Tables 4(a)–4(e)). The bulk post-weld slag analyses are also shown in each table to enable comparison to the glass phase SEM analyses. In slag samples from fluxes 1 to 4, a fluoride-silicate crystallisation phase formed as differently shaped crystals precipitated from the liquid matrix upon cooling, to form the primary solidification phase (PSP). These phases can be seen in different morphology appearances in the SEM BSE (Back Scattered Elec-

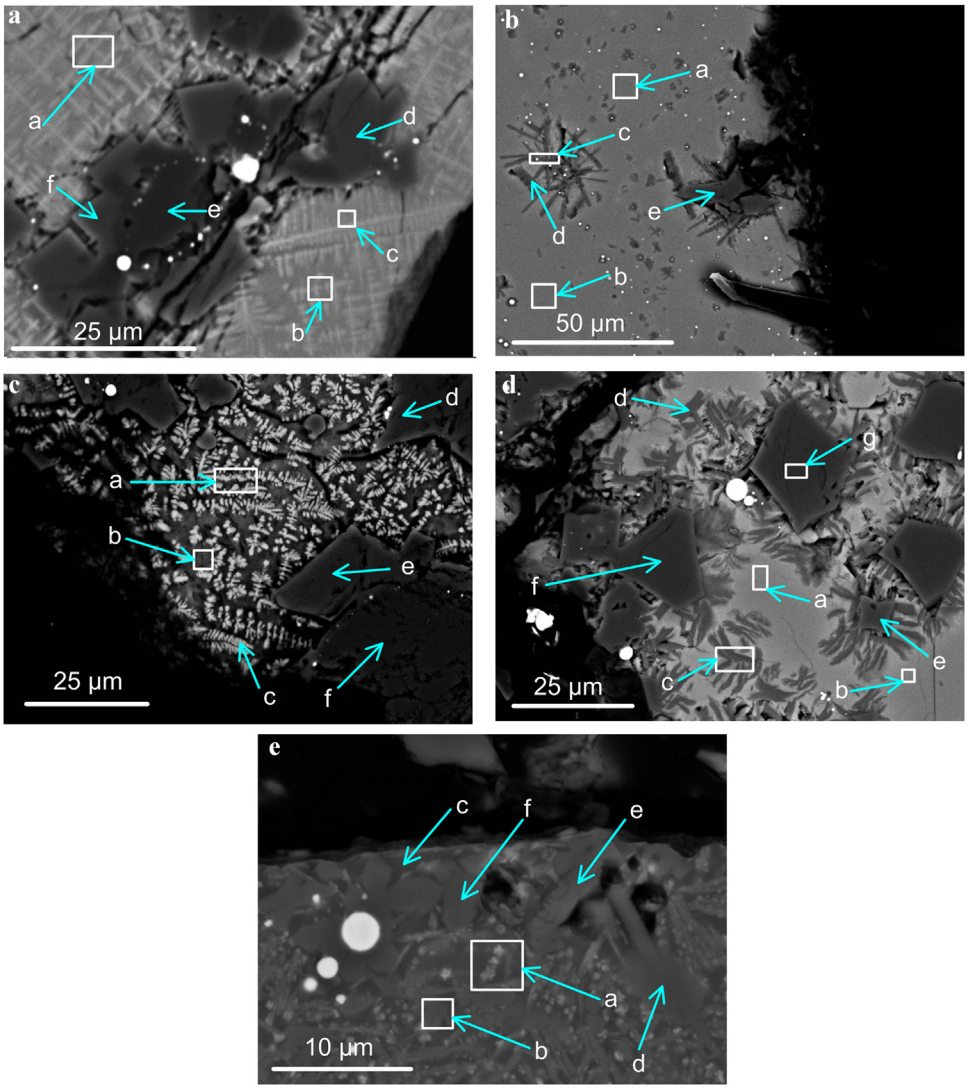

Fig. 3 – (a) Slag-metal interface slag BSE image for Flux 1 (×2000). (b) Slag-metal interface slag BSE image for Flux 2 (×900). (c) Slag-metal interface slag BSE image for Flux 3 (×1400). (d) Slag-metal interface slag BSE image for Flux 4 (×1200). (e) Slag-metal interface slag BSE image for Flux 5 (×4000).

Table 4(a) – SEM analyses of phases in Fig. 3(a): (mass%).

4(a)	a Glass[a]	b Glass	c Dendrites	d Spinel	e MgO	f Spinel	Bulk slag
O	26.1	28.1	32.3	46.0	38.9	45.6	31.6
Al	2.4	2.0	2.1	33.1	0	32.6	7.4
Mn	1.0	1.0	0.9	0.6	0	0.7	0.9
Mg	11.0	11.6	11.6	18.1	59.9	19.4	20.3
Ti	0	0	0	1.3	0	0.9	0.4
Si	9.6	10.1	9.1	0.8	0	0.6	7.1
Fe	0	0	0	0	1.1	0	1.8
Ca	24.9	24.5	26.4	0.2	0.1	0.2	17.2
Na	1.9	1.8	1.9	0	0	0	0.5
K	0.8	0.7	0.7	0	0	0	0.6
F	22.3	20.2	15.5	0	0	0	11.5
Total	100.0	100.0	100.0	100.0	100.0	100.0	99.3

[a] Glass = liquid matrix phase.

Table 4(b) – SEM analyses of phases in Fig. 3(b): (mass%).

4(b)	a Glass	b Glass	c PSP[a]	d PSP	e Spinel	Bulk slag
O	34.1	33.7	34.5	36.2	44.9	33.3
Al	9.4	9.2	9.5	8.7	32.9	9.3
Mn	3.9	3.7	3.2	3.5	2.8	4.3
Mg	12.3	12.7	13.0	12.6	16.6	13.2
Ti	1.0	1.0	1.0	1.0	1.8	1.1
Si	9.8	10.1	9.8	9.1	0.6	10.0
Fe	0.4	0	1.0	0.2	0.3	2.1
Ca	13.4	13.3	10.8	13.4	0.1	14.2
Na	1.8	1.9	3.1	3.3	0	1.1
K	1.0	1.0	1.3	0.8	0	1.2
F	12.9	13.4	12.8	11.2	0	9.6
Total	100.0	100.0	100.0	100.0	100.0	99.4

[a] PSP = primary solidification phase.

Table 4(c) – SEM analyses of phases in Fig. 3(c): (mass%).

4(c)	a Glass	b Glass	c Dendrites	d Spinel	e Spinel	f MgO	Bulk slag
O	20.5	33.5	14.3	46.1	45.9	39.6	30.8
Al	2.5	3.5	2.0	32.2	33.5	0	8.9
Mn	0.9	1.3	0.7	0.9	0.8	0.8	1.2
Mg	5.8	10.2	5.4	18.2	17.6	57.8	17.4
Ti	0.4	0.6	0	1.8	1.5	0	0.7
Si	6.8	11.4	6.1	0.6	0.6	0	6.2
Fe	0	0.2	0.2	0	0	1.8	2.8
Ca	28.9	23.7	26.8	0.2	0.1	0	18.2
Na	1.1	1.7	1.1	0	0	0	0.8
K	0.9	1.4	0.7	0	0	0	0.9
F	32.2	12.5	42.7	0	0	0	11.9
Total	100.0	100.0	100.0	100.0	100.0	100.0	99.8

Table 4(d) – SEM analyses of phases in Fig. 3(d): (mass%).

4(d)	a Glass	b Glass	c Glass + PSP[a]	d PSP	e Spinel	f Spinel	g Spinel	Bulk slag
O	34.3	34.1	36.1	37.5	45.5	46.1	45.7	36.1
Al	6.8	6.2	6.7	7.5	35.7	35.2	35.4	13.7
Mn	5.7	5.8	4.5	2.4	1.9	2.1	2.1	5.0
Mg	12.4	12.3	15.9	15.2	15.9	15.9	16.1	14.1
Ti	0.6	0.7	0.7	0.6	0.2	0.2	0.3	0.6
Si	12.1	12.4	12.7	13.0	0	0	0	9.2
Fe	0.7	0.5	0.4	0.3	0.8	0	0.4	3.4
Ca	12.8	13.3	8.2	8.2	0	0	0	9.0
Na	2.0	2.0	2.4	2.8	0	0	0	0.2
K	0.3	0	0.3	0.4	0	0	0	0.2
F	12.3	12.7	12.1	12.1	0	0	0	7.0
Total	100.0	100.0	100.0	100.0	100.0	100.0	100.0	98.5

[a] PSP = primary solidification phase.

tron) images of the slags at the slag-metal interface (Fig. 3): as dendrites in Fig. 3(a), (c) and (e), as needles in Fig. 3(b) and as feather shaped phases in Fig. 3(d). In the slags from fluxes 1 and 3, in Fig. 3(a) and (c), these dendrites were densely distributed so that the liquid matrix was analysed as area analysis to include the dendrite phase at positions (a) and (b) in Fig. 3(a) and at position (a) in Fig. 3(c). In fluxes 2 and 4, in Fig. 3(b) and (d), the crystallisation phases were smaller in number and the liquid matrix phase could be analysed separately from the crystallisation phase. Due to the low fluoride content in flux 5 the fluoride was incorporated completely into the liquid matrix phase. The finely intergrown solidification crystals observed in flux 5, see position (a) in Fig. 3(e), were most likely part of a homogenous slag at the welding temperatures.

4. Discussion

The solid crystalline phases present in the polished sections displayed in Fig. 3(a)–(e) may have formed as cooling phases as the post-weld slag cooled down from high weld-

Table 4(e) – SEM analyses of phases in Fig. 3(e): (mass%).

4(e)	a Area	b Area	c Glass	d Spinel	e Spinel	f Spinel	Bulk slag
O	44.8	44.6	46.0	48.0	46.4	47.3	40.1
Al	19.8	25.6	13.5	26.8	30.8	30.7	20.4
Mn	6.4	9.4	3.8	8.6	8.8	8.4	9.1
Mg	2.5	4.8	1.5	6.3	8.4	8.4	3.2
Ti	7.4	4.9	4.0	4.0	2.4	2.4	6.7
Si	7.2	4.4	12.5	3.4	1.8	1.7	7.9
Fe	0.3	0	0.2	0.4	0.5	0	3.9
Ca	2.2	2.2	3.3	1.7	0.4	0.4	4.0
Na	3.5	0.9	7.5	0.6	0.5	0.6	0.4
Zr	0.7	0	1.6	0	0	0	1.5
K	0.4	0.3	0.8	0.2	0	0.1	0.4
F	3.8	1.9	5.3	0	0	0	1.8
Total	100.0	100.0	100.0	100.0	100.0	100.0	99.4

ing temperatures of 2000 °C–2500 °C in the arc column to room temperature [10,11]. This possibility was investigated by plotting the phase cooling curves for each flux composition by using the Equilib module in FactSage 6.4. Although there are no published multi-component phase diagrams available for the $CaO–SiO_2–MgO–Al_2O_3–CaF_2$ system, the FactSage thermochemical software calculation outputs were confirmed to be accurate compared to some equilibrated slag samples as reported in a previous study [22]. Therefore the FactSage calculations in this study are used with confidence.

The calculation results are displayed in Fig. 4(a)–(e), and confirm that the solid phases seen in Fig. 3(a)–(e) are cooling phases since the bulk flux was completely liquid at the process welding temperature of 2000 °C in the weld pool [23,24]. According to the equilibrium cooling curves in Fig. 4(a) and (c) fluxes 1 and 3 should form spinel and monoxide solid phases upon equilibrium cooling. Spinel and monoxide phases were identified in both fluxes as indicated in Fig. 3(a) and (c). Similarly, the cooling curves for fluxes 2 and 4 indicate that only spinel phase should form on cooling. This was also the observation from Fig. 3(b) and (d). The phase assembly in Fig. 3(e), for flux 5, appears to be complicated. The only clear solid phase identification was made for the spinel phase, and this is in agreement with the cooling curve for flux 5 displayed in Fig. 4(e) as a titanium containing spinel phase. The corundum phase shown in the cooling curve was not identified in Fig. 3(e).

The bulk flux liquidus temperatures as indicated by the cooling curves in Fig. 4(a)–(e) for fluxes 1–5 are 1732 °C, 1621 °C, 1673 °C, 1732 °C and 1593 °C which is clearly a wide range of liquidus temperatures considering SAW processing temperatures range from high arc cavity temperatures (2000 °C–2500 °C) to approximately 50 °C below the solidification temperature of the welded steel plate (typically 1480 °C for High Strength Low Alloy steels) [10,11,25]. The reason for this aim solidification temperature is that the slag should solidify after the weld pool steel has solidified so that a maximum quantity of oxide inclusions may float out of the weld pool (steel) and be absorbed into the molten slag layer at the slag-weld pool interface, to ensure clean steel in the weld metal.

This liquidus lowering effect of CaF_2 is illustrated by comparing the cooling curve of each flux in the absence of CaF_2, as displayed in Fig. 5(a)–(e), to the complete flux composition based cooling curves as displayed in Fig. 4(a)–(e). Although fluxes 1–3 contain similar quantities of CaF_2, the liquidus lowering effect of CaF_2 in fluxes 1 and 3 (of similar composition) is much higher at 19 °C/%CaF_2 compared to its liquidus lowering effect in flux 2 at only 4 °C/%CaF_2. Flux 4 contains somewhat less CaF_2 at 18 mass%, but the effect of this CaF_2 addition on the liquidus temperature is similar to that in flux 2 at 4 °C/%CaF_2. In flux 5 the flux liquidus temperature is already relatively low at 1595 °C, see Fig. 5(e), with 4% CaF_2 addition it is only lowered slightly to 1593 °C. Therefore, addition of CaF_2 is likely primarily motivated by a different formulation requirement than the lowering of the liquidus temperature in flux 5.

A better visualisation of the flux formulation basis (excluding CaF_2) may be viewed from Fig. 6(a) for fluxes 1–4 and Fig. 6(b) for flux 5. The composition plots were made by summing CaO, MgO and MnO since these oxides easily substitute for each other in the monoxide phase. Fig. 6(a) illustrates that fluxes 1 and 3 project onto the same line of MgO/SiO_2 at very similar overall compositions, although these two fluxes were sourced from two different supply companies and one of these describe this flux as neutral with respect to Mn and Si transfer from the slag to the weld metal. Similarly, fluxes 2 and 4 were also sourced from these two different companies and appear to be somewhat similar in chemistry in terms of the MgO/SiO_2 line in Fig. 6(a). The lower ratio of MgO/SiO_2 accords with the supplier description of flux 4 as a low Si pickup flux. Therefore, the higher SiO_2 content in this flux should result in an increased SiO_2 activity in the slag and thus enhance Si transfer from the slag to the weld metal. This flux is also described as a medium Mn pickup flux since it contains more MnO (~6 mass% MnO) compared to the Mn-neutral fluxes 1 and 3 at ~1 mass% MnO. In Fig. 6(a) the equivalent composition of flux 5 is displayed as well and it appears to plot close to the same MgO/SiO_2 line as fluxes 2 and 4. However, flux 5 contains a significant quantity if TiO_2 and therefore a separate pseudo-ternary diagram is used to plot this composition, see Fig. 6(b), indicating a lower liquidus temperature for this composition point compared to that in Fig. 6(a). Therefore, addition of TiO_2 to the $SiO_2–MgO–Al_2O_3$ system composition point for flux 5 appears to lower the liquidus temperature significantly as illustrated from comparison of the flux 5 points in Fig. 6(a) vs. (b).

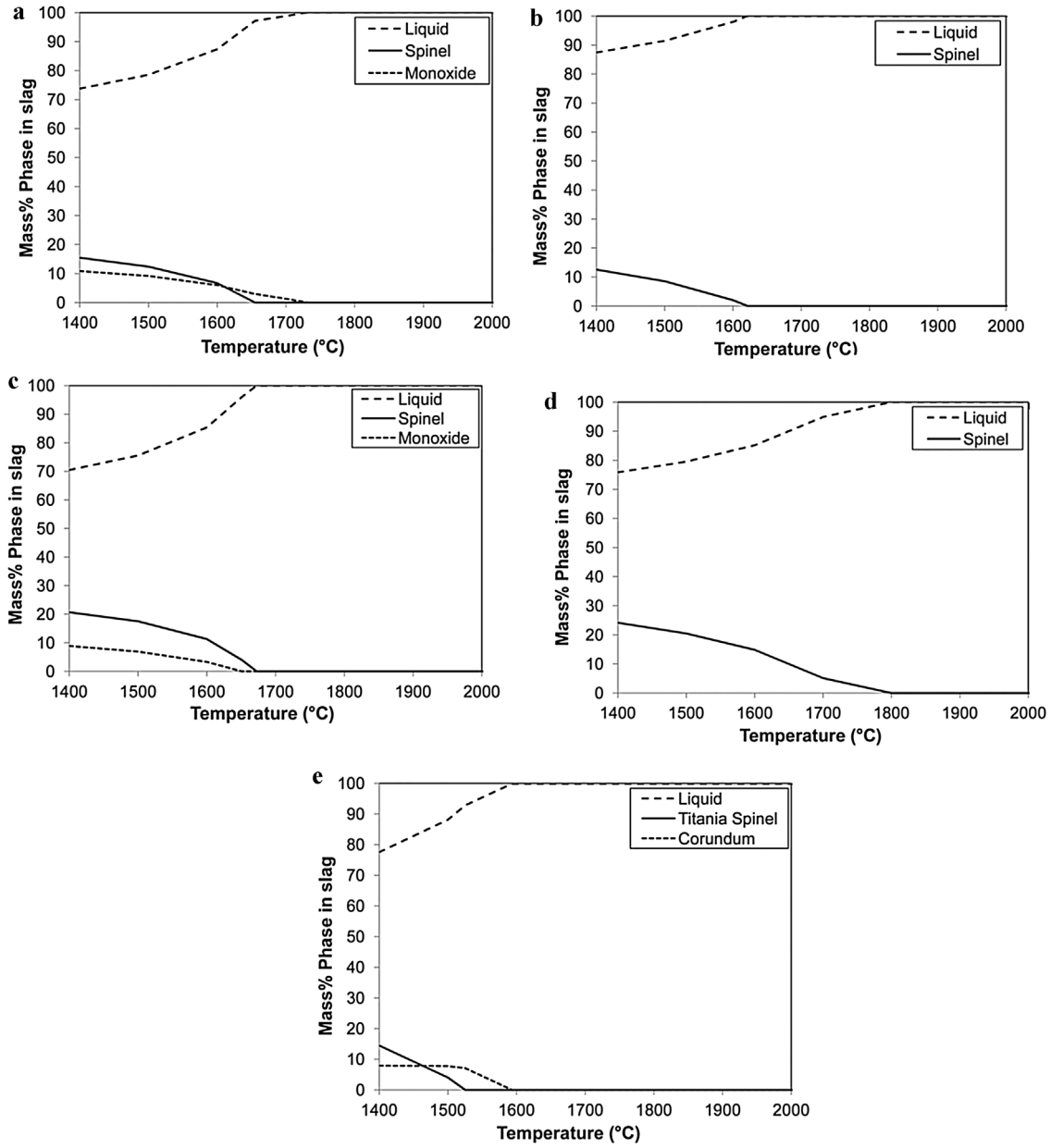

Fig. 4 – (a) Flux 1 phase chemistry vs. temperature. (b) Flux 2 phase chemistry vs. temperature. (c) Flux 3 phase chemistry vs. temperature. (d) Flux 4 phase chemistry vs. temperature. (e) Flux 5 phase chemistry vs. temperature.

Table 5 – Major gas phase compounds calculated from slag-gas equilibrium in FactSage (volume percentages).

Flux number	1	2	3	4	5
MgF_2	11	27	16	39	3
CaF_2	11	22	16	18	2
AlF_3	1	6	1	15	36
NaF	45	21	30	14	10
KF	28	15	31	3	18
$NaAlF_4$	1	5	2	8	14
SiF_4	0	0	0	0	4
Na	3	1	2	1	0
TiF_3	0	0	0	0	7
Total	98	98	98	97	94
g gas/100 g flux	2	12	4	9	3

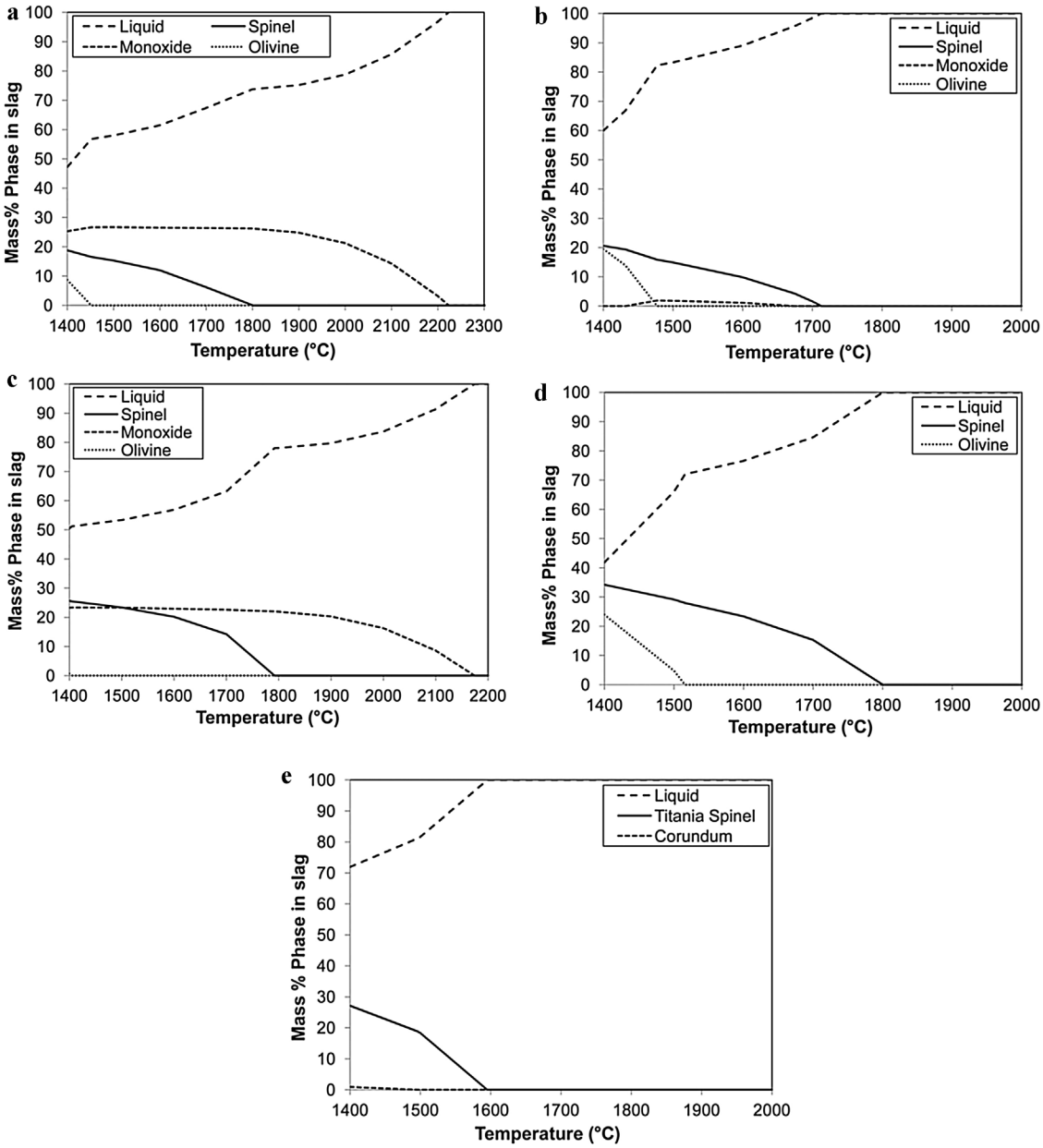

Fig. 5 – (a) Flux 1 phase chemistry vs. temperature (CaF_2 removed). (b) Flux 2 phase chemistry vs. temperature (CaF_2 removed). (c) Flux 3 phase chemistry vs. temperature (CaF_2 removed). (d) Flux 4 phase chemistry vs. temperature (CaF_2 removed). (e) Flux 5 phase chemistry vs. temperature (CaF_2 removed).

Since the fluoride added to the flux is incorporated into the slag liquid phase and not into any of the solid phases observed in Fig. 3(a)–(e), and solid phases are absent from the slag at the SAW processing temperatures, it is expected that additional underlying considerations must be of importance in setting CaF_2 additions levels in flux chemistry formulations. To this end the flux formulations were considered in terms of fluoride gas species formation as discussed in the following section. FactSage calculations were used to better explain the tendency of fluoride gas formation from each flux. The gas-slag equilibrium was calculated at 2200 °C for each flux composition by using the Equilib module. This temperature was selected with reference to the typical arc cavity temperatures of 2000 °C–2500 °C reported in literature [10,11].The major gas phase compounds so calculated are summarised in Table 5. It is seen that fluxes 1 and 3 are expected to form similar quantities of gas of similar composition since these two fluxes are similar in bulk chemical composition. NaF and KF are the main gas compounds and smaller quantities of MgF_2 and CaF_2 are predicted in the gas phase for flux 1 and 3. In flux 2 and 4, formation of mostly the same major gas compounds as in flux 1 and 3 are predicted, but AlF_3 is formed to a larger extent and KF to a lesser extent. For flux 5 the main gas compound predicted is AlF_3 since Al_2O_3 is the main compound in this flux. Large quantities of $NaAlF_4$ may also form in flux 5, and some NaF and KF may form. Thus, it appears from

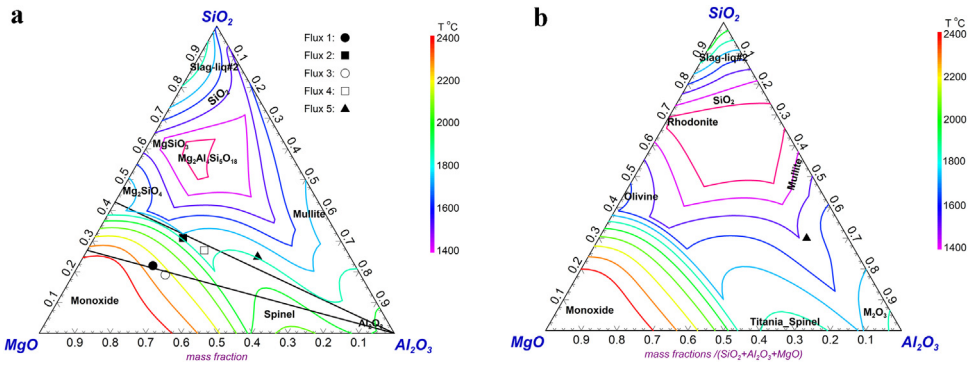

Fig. 6 – (a) SiO_2–MgO–Al_2O_3 phase diagram liquidus projection (fluxes 1–5). (b): SiO_2–MgO–Al_2O_3–TiO_2–MnO pseudo-ternary phase diagram liquidus projection (flux 5); Z = (SiO_2 + Al_2O_3 + MgO), TiO_2/Z = 0.17226, MnO/Z = 0.19802.

Table 5 that flux formulations are most likely made with consideration of the quantity and type of fluoride gas compound formation, in addition to parameters such as slag liquidus temperature, slag viscosity and slag component activity levels.

It is not clear how the initial addition of CaF_2 to each flux is transformed to the different fluoride gas compounds shown in Table 5. Therefore, Gibbs free energy calculations were made to investigate the relative stability of these fluoride gas compounds relative to CaF_2. Although fluoride is usually added as CaF_2, it can react with various oxides to different extents with the result that flux formulations should take this type of reaction into consideration [26]. Reaction of CaF_2 with flux oxide compounds of the type shown in reaction (1) was considered for various oxides to calculate the Gibbs free energy for each reaction to form one mole product fluoride gas. The following input parameters were used in the reaction module of FactSage 6.4: for each reaction the CaF_2 partial pressure was set to 0.5 atm.; the product fluoride gas partial pressure was set to 0.10 atm.; the activity of the flux oxide was set to unity and the activity of CaO set to 0.01 (a_{CaO} = 0.01). The calculation results are illustrated Fig. 7.

$$SiO_2(l) + 2CaF_2(g) \leftrightarrow 2CaO(s) + SiF_4(g) \quad (1)$$

Clearly, the fluorides of K and Na form most easily at typical SAW temperatures. This observation is agreement with the predicted gas phase analyses in Table 5, showing substantial proportions of NaF and KF in the gas phase for all the fluxes. This is important since alkali metal oxides were reportedly added to flux to ensure a stable arc [27]. Formation of KF and NaF may be important to ensure decreased levels of loss of K and Na in the form of easily volatilised K(g) and Na(g), by forming the fluorides instead of volatilised elements, K and Na. Also important is that FeF_3(g) should form less easily since iron should remain in the weld metal and not be lost in significant quantities to gas or slag.

In terms of the other important element in the weld metal, manganese, the thermodynamic data does not show MnF_2 and MnF_3 as gasses, only as solids or liquids. However, manganese does easily volatilise as Mn(g) and therefore MnO is added to flux to counter this manganese loss, and the partial pressure

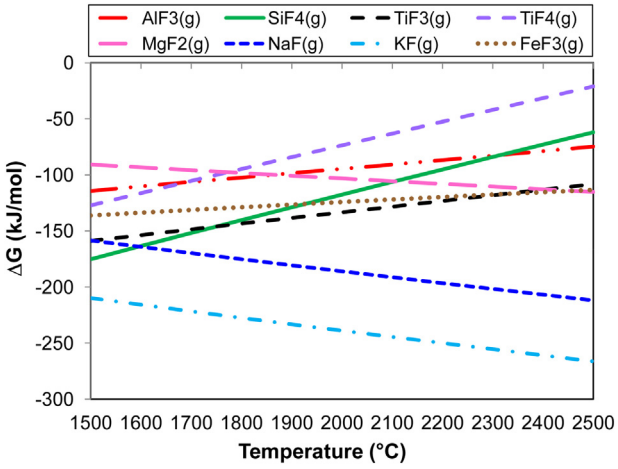

Fig. 7 – Gibbs free energy values of reaction type (1) at P_{CaF2} = 0.50 atm; P_{XF} = 0.10 atm, reactant oxide activities = 1.0; a_{CaO} = 0.01.

of Mn(g) in the arc cavity will be influenced by the presence of the fluoride gasses formed from other element oxides.

In Fig. 7, the line for MgF_2(g) formation crosses that for TiF_4(g) formation at ~1800 °C, indicating the relatively higher likelihood of loss of MgO from the flux to the gas phase as MgF_2(g) than the loss of TiO_2 as TiF_4(g). Similarly, the MgF_2(g) formation line crosses the SiF_4(g) line at ~2150 °C. Therefore, MgO may be added to the flux to be formed into a fluoride gas instead of TiF_4(g) and SiF_4(g). As indicated in Fig. 7, the oxidation state of titanium in its oxides will be an important factor in setting the quantity of titanium volatilized as fluoride gas, with TiF_3(g) more easily volatilized. This appears to be an important factor since the main titanium-fluoride gas compound in Table 5 is TiF_3(g). According to the data plot in Fig. 7, formation of AlF_3(g) is thermodynamically less favourable than MgF_2(g) formation at temperatures above ~1900 °C, and also less favourable than SiF_4(g) formation at temperatures below ~2300 °C. Comparison of this information to the more complex calculated data in Table 5, which shows AlF_3(g) as the main gas compound predicted from flux 5 chemistry, indicates that the relative activity of oxide compounds in the flux

is important in flux chemistry formulation to form specific fluoride compounds. Therefore, the relative ease of fluoride gas formation from reactions similar to reaction (1) for the different flux oxides is important in flux formulations to transfer targeted elements such as titanium and silicon from the slag to the weld metal.

5. Conclusions

- The chemical formulation of fluoride based commercial agglomerated SAW fluxes (Fluoride Basic flux, Aluminate Basic flux and Aluminate Rutile flux) is based on the SiO_2–Al_2O_3–MgO ternary slag system, with varying additions of CaF_2.
- The solids phases observed in the slag microstructures at the weld metal-slag interface formed as cooling phases, and the slag was fully molten at the SAW processing temperatures of 2000 °C–2500 °C.
- FactSage thermochemical calculations were used to quantify the extent of slag liquidus temperature lowering by CaF_2 addition as 19 °C/%CaF_2 in fluxes 1 and 3; 4 °C/%CaF_2 in fluxes 2 and 4.
- The extent of CaF_2 addition to fluxes to ensure formation of different fluoride gas compounds to shield the weld pool from oxygen, nitrogen and hydrogen pickup was explored and explained by using thermochemical calculations.

Conflicts of interest

The authors declare no conflicts of interest.

Funding

This work was supported by the National Research Foundation (NRF) of South Africa (BRIC171211293679).

REFERENCES

[1] Palm HJ. How fluxes determine the metallurgical properties of submerged arc welds. Weld J 1972;51:358S–60S.
[2] Tuliani SS, Boniszewski T, Eaton NF. Notch toughness of commercial submerged arc weld metal. Weld Met Fabr 1969;37:327–39.
[3] Eagar TW. Sources of weld metal oxygen contamination during Submerged Arc Welding. Weld J 1978;57:76S–80S.
[4] Chai CS, Eagar TW. The effect of SAW parameters on weld metal chemistry. Weld J 1980;59:93S–8S.
[5] Chai CS, Eagar TW. Slag metal reactions in binary CaF_2-metal oxide welding fluxes. Weld J 1982;61:229S–32S.
[6] Du Plessis J, Du Toit M, Pistorius PC. Control of diffusible weld metal hydrogen through flux chemistry modification. Weld J 2007;86:273S–80S.
[7] Burck PS, Indacochea JE, Olsen DL. Effects of welding flux additions on 4340 steel weld metal composition. Weld J 1990;69:115S–22S.
[8] Park J-Y, Chang W-S, Sohn I. Effect of MnO to hydrogen dissolution in CaF_2-CaO-SiO_2 based welding type fluxes. Sci Technol Weld Join 2012;17:134–40.
[9] Kumar A, Singh H, Maheshwari S. A review study of Submerged Arc Welding fluxes i-manager's. J Mech Eng 2013;3:44–52.
[10] Mitra U, Eagar TW. Slag-metal reactions during welding: part II. Theory. Metall Trans B 1991;22:73–81.
[11] Mitra U, Eagar TW. Slag-metal reactions during welding: part III. Verification of the theory. Metall Trans B 1991;22:83–100.
[12] Polar A, Indacochea JE, Blander M. Electrochemically generated oxygen contamination in Submerged Arc Welding. Weld J 1990;69:68S–74S.
[13] Lau T, Weatherly GC, Mc Lean A. The sources of oxygen and nitrogen contamination in Submerged Arc Welding using CaO-Al_2O_3 based fluxes. Weld J 1985;69:343S–7S.
[14] Mitra U, Eagar TW. Slag metal reactions during Submerged Arc Welding of alloy steels. Metall Trans A 1984;15:217–27.
[15] Indacochea JE, Blander M, Christensen N, Olson DL. Chemical reactions during Submerged Arc Welding with FeO-MnO-SiO_2 fluxes. Metall Trans B 1985;16:237–45.
[16] Baunè E, Bonnet C, Liu S. Reconsidering the basicity of a FCAW consumable-Part 1: solidified slag composition of a FCAW consumable as a basicity indicator. Weld J 2000;79:57S–65S.
[17] Kim JB, Lee TH, Sohn I. Effect of compositional variation in TiO_2-based Flux-Cored Arc Welding fluxes on the thermo-physical properties and mechanical behavior of a weld zone. Metall Trans A 2018;49:2705–20.
[18] Jastrzebska I, Szczerba J, Stoch P, Prorok R, Sniezek E. Effect of electrode coating type on the physico-chemical properties of slag and welding technique. Biul Inst Spaw 2015;56:37–46.
[19] Paniagua-Mercado AM, Estrada-Diaz P, Lopez-Hirata VM. Chemical and structural characterization of the crystalline phases in agglomerated fluxes for submerged-arc welding. J Mater Process Technol 2003;141:93–100.
[20] Sharma S, Kumar J, Chhibber R. Experimental investigation on surface behaviour of Submerged Arc Welding fluxes using basic flux system. Ceram Int 2020;46:8111–21.
[21] Bale CW, Chartrand P, Degterov SA, Eriksson G. FactSage thermochemical software and databases. CALPHAD 2002;26:189–228.
[22] Park JH. Solodification structure of CaO-SiO_2-MgO-Al_2O_3 (-CaF_2) systems and computational phase equilibria: crystallization of $MgAl_2O_4$ spinel. CALPHAD 2007;31:428–37.
[23] Chai CS, Eagar TW. Slag-metal equilibrium during Submerged Arc Welding. Metall Trans B 1981;12:539–47.
[24] Mitra U, Eagar TW. Slag-metal reactions during welding: part 1. Evaluation and reassessment of existing theories. Metall Trans B 1991;22:65–71.
[25] Singh B, Khan ZA, Siddiquee AN. Effect of flux composition on element transfer during Submerged Arc Welding (SAW): a literature review. Int J Curr Res 2013;5:4181–6.
[26] Lau T, Weatherly GC, Mc Lean A. Gas/metal/slag reactions in Submerged Arc Welding using CaO-Al_2O_3 based fluxes. Weld J 1986;70:31S–8S.
[27] Kohno R, Takami T, Mori N, Nagano K. New fluxes of improved weld metal toughness for HSLA steels. Weld J 1982;61:373S–80S.